Delft University of Technology

Performance Comparison between Data Centers with Different Airflow Management Technologies

Li, Xueqiang; Zhang, Zhongyao; Wang, Qihui; Yang, Xiaohu; Hooman, Kamel; Liu, Shengchun

Important note
To cite this publication, please use the final published version (if applicable).
Please check the document version above.

Performance Comparison between Data Centers with Different Airflow Management Technologies

Xueqiang Li, Zhongyao Zhang, Qihui Wang, Xiaohu Yang, Kamel Hooman & Shengchun Liu

Published online: 15 Jul 2023.

Submit your article to this journal ⬀

View related articles ⬀

View Crossmark data ⬀

Taylor & Francis
Taylor & Francis Group

Check for updates

Performance Comparison between Data Centers with Different Airflow Management Technologies

Xueqiang Li[a], Zhongyao Zhang[a], Qihui Wang[a], Xiaohu Yang[b], Kamel Hooman[c], and Shengchun Liu[a,d]

[a]Key Laboratory of Refrigeration Technology of Tianjin, Tianjin University of Commerce, Tianjin, China; [b]Institute of Building Environment and Sustainability Technology, School of Human Settlements and Civil Engineering, Xi'an Jiaotong University, Xi'an, China; [c]Department of Process and Energy (P&E), Delft University of Technology, Delft, Nederland; [d]Key Laboratory of Efficient Utilization of Low and Medium Grade Energy, Tianjin University, China

ABSTRACT

Air cooling systems are widely used in current data centers owing to their low capital costs and high reliability. To satisfy the increasing rack power density, the optimal air-cooling technology and an economic analysis should be carefully discussed. Therefore, this study discusses four airflow management technologies: Case 1: raised floor and cold aisle containment supply/computer room air conditioning (CRAC) direct return; Case 2: CRAC direct supply/hot aisle containment (HAC) return; Case 3: overhead duct supply/CRAC direct return; and Case 4: overhead duct supply/HAC return. Using a validated model, the thermal and economic performances of each case were compared. Results showed that Case 4 exhibited the best thermal performance, followed by Cases 3, 2, and 1. Case 1 cannot satisfy the heat dissipation requirement when the rack power density is larger than 12.5 kW; whereas only Case 4 can be used when the power density is larger than 15 kW. Regarding location within China, owing to the high ambient temperature, Shenzhen showed the highest annual cost value and power usage effectiveness, followed by Shanghai, Xi'an, Beijing, and Harbin. Finally, Cases 3 and 4 are recommended for application when the rack power density is greater than 10 kW.

Introduction

With the development of cloud computing, 5 G, and network technology, the energy consumption of data centers (DCs) has increased sharply, negatively impacting the environment [1, 2]. Reducing energy consumption is extremely urgent to meet the requirements of "peak carbon dioxide emissions" and "Carbon neutrality" [3]. It is estimated that the energy consumption of DCs would be as high as 13% of the global power generation by 2030 [4], of which approximately 30%–60% of the electricity would be used for refrigeration systems [5]. Therefore, DC design and operation optimization are crucial for saving energy in DCs.

To reduce energy consumption, many efforts have been dedicated to study the performance of new technologies, such as liquid [6], two-phase [7], and integrated cooling systems [8]. Although these new technologies could largely improve the cooling efficiency and reduce energy consumption, the capital,

operational, and maintenance costs as well as the payback period need to be further considered. Therefore, the information and communications technology industry still prefer an air cooling system until acoustic noise and thermal requirements cannot longer be met [9].

Therefore, optimizing the air-cooling system in DCs for energy consumption reduction has received considerable attention [10]. The existing related literature can be divided into two categories. One is related to thermal performance optimization based on a specific structure. Wang et al. [11, 12] studied the performance of airflow management by combining an overhead air supply system with cold aisle containment (CAC). It was found that the above structure could exhibit a high rack-cooling index of 99%. The other category relies on the thermal performance comparison between different airflow management technologies. For instance, Abbas et al. [13] found that in-row cooling was better for rack power densities of less than 10 kW, while perimeter cooling was

Nomenclature

A	Area, m^2		SHI	Supply heat index
ACV	Annual cost value		t_{total}	Annual working time of the refrigeration system, h
b	Basic rate of return		T	Temperature, °C
c_p	Constant pressure specific heat capacity, kJ/(kg·°C)		T_P	Temperature of the porous matrix, °C
C	Cost, CNY		T_f	Temperature of the fluid flowing through the matrix, °C
CAC	Cold aisle containment		u	x-direction velocity, m/s
CNY	Chinese Yuan		v	y-direction velocity, m/s
CRAC	Computer room air conditioner		V	Air volume flow, m^3/s
D	Diameter, m		w	z-direction velocity, m/s
DC	Data center		W	Width, m
E	Energy consumption, kW·h			
E_{IT}	Rack energy consumption, kW·h			
f	Average electricity price, kW·h/CNY		**Greek symbols**	
FC	Free cooling		γ	Heat transfer coefficient, W/(m^2·°C)
g	Gravitational acceleration, m/s^2		δQ	Enthalpy increase, kW
h	Enthalpy, kJ/kg		δ_{ij}	Kronecker delta function
H	Height, m		η	Load rate, %
HAC	Hot aisle containment		μ	Dynamic viscosity, Pa·s
k	Thermal conductivity, W/(m·°C)		ρ	Density, kg/m^3
K_T	Temperature inequality index		$\Phi 0$	Refrigerating capacity, kW
L	Length, m			
m	Economic life, years		**Subscripts**	
$\dot{m}$	Mass flow, kg/s		amb	Ambient
M	Air mass flow, kg/s		avg	Average
n	Numbers		CS	Cooling system
P	Pressure, Pa		con	Construction
P_{com}	Energy consumption of compressor, kW		ES	Electrical systems
PUE	Power usage effectiveness		i	Row number
q	Mass flow in refrigeration system, kg/s		in	Rack inlet
Q	Heat dissipation, kW		j	Column number
Q_H	Heat source per unit volume, W		max	Maximum
R	Resistance vector of the porous media		min	Minimum
RHI	Return heat index		op	Operation
S	Source term		out	Rack outlet
SAT	Supply air temperature, °C			

only suitable for rack power densities of less than 5 kW. Moreover, free-cooling (FC) technology can be used to cool DCs when the ambient temperature is low [14]. Ham and coworkers [15, 16] found that air- and water-side economizers could reduce the energy consumption by up to 67.2% and 24%, respectively. Additional literature on DC thermal performance can be found in Table 1 [11–13, 17–27].

From Table 1, it is clear that although many studies have been conducted to improve the thermal performance, most of them have a rack power density of less than 10 kW. For a high-power rack density, the relative work is insufficient. The main differences arise from two aspects: (1) Which kind of airflow management could be employed and what is its thermal performance? (2) If airflow management is employed for a high-power rack density, what is the economics? To fill this knowledge gap, this study compared four types of airflow management technologies that are normally used in the current DCs. The four airflow management technologies are the following: Case 1: raised floor and CAC supply/computer room air conditioning

(CRAC) direct return; Case 2: CRAC direct supply/hot aisle containment (HAC) return; Case 3: overhead duct supply/CRAC direct return; and Case 4: overhead duct supply/HAC return. With a validated three-dimensional (3D) model, the thermal performance was first compared when the rack power density ranged from 5 to 15 kW. The economic performance of these four technologies was then compared with respect to FC technology in different cities in China. The conclusions obtained in this study could provide guidance for upgrading and selecting airflow management technologies for current and future DCs.

Models and methods

DC Description

In a DC room, airflow management is crucial to the performance of internet technology equipment. Four different airflow management technologies were designed, as shown in the 2D and 3D schematics presented in Figure 1. The rack configuration was the

Table 1. Existed work about airflow management technology in data center.

Research type	Authors	Rack power density (kW)	Content	Key findings
Optimization	Wang et al. [11, 12]	3	Overhead duct supply	Large air flow rate and the blockage was helpful to improve the efficiency index.
	Zhang et al. [17]	1.94	Height of raised floor	They suggested the height of raised floor, CAC, and HAC are 1.0–1.2 m, 0.6–0.8 m, and 0.4–0.6m, respectively.
	Nada et al. [18]	0.6	Porosity of perforated tiles.	Perforated tiles with 25% of porosity was suggested when the rack power density was less than 5 kW.
	Fulpagare et al. [19]	10	Effect of obstructions and plenum chamber.	Obstructions in the plenum chamber could largely decrease air flow rates, leading to hot spot of rack.
	Nada et al. [20–22]	3.5–7	Layout of CRAC and racks.	CRAC perpendicular to racks could improve air distribution uniformity and reduce the hot air circulation.
	Chu et al. [23]	5	Overhead duct supply and air flowrate	Hot air circulation can be avoided when flow rate of cold air in rack was larger than that of DC room air handler.
Comparison	Srinarayana et al. [24]	5	Ceiling return with vents Ceiling return with ducts Ceiling supply with room return	Compared to room return, ceiling return strategy for hot air return showed a better thermal performance of the DC, for both raised- and non-raised-floor strategy.
	Nemati et al. [25]	6.8	CAC return, HAC return, and overhead duct return.	HAC return and overhead duct return had higher startup time
	Zhan et al. [26]	5.7	HAC return with different diffuser.	In the best case, the diffuser is able to supervise the average rack temperature by 8.56 °C.
	Shrivastava et al. [27]	8.7	CAC supply, HAC return and overhead duct return.	HAC return could reduce energy consumption and power usage effectiveness (PUE) up to 40% and 13%, respectively.
	Abbas et al. [13]	3.5–10	In-row cooling and raised floor cooling	In-row cooling was better for rack power density less than 10 kW and raised floor cooling was only suitable for rack power density less than 5 kW.

same; the racks were arranged in four rows. Each row contained 14 racks. The power density of each rack was varied from 5 to 15 kW. CRAC was used to provide cooled air. The internal fans are arranged on the rack inlet, where the number of fans is 5×2 for one rack.

For Case 1 (raised floor and CAC supply/CRAC direct return), the raised floor was used, CAC was formed between two adjacent rack rows, and CRACs were distributed on both sides of the DC room. During operation, cold air is transferred to the CAC through the perforated tile. Hot air from the rack was suctioned by the CRAC, as shown in Figure 1a. For Case 2 (CRAC direct supply/HAC return), shutters on the partition wall are used, in which the plenum chamber can be formed to distribute the cold air more uniformly. HAC was formed between two adjacent rows, it was also connected to the ceiling to form the return channel, as shown in Figure 1b. For Case 3 (overhead duct supply/CRAC direct return), the overhead duct was used for the air supply, which can transfer cold air to every rack. Hot air was suctioned by the CRAC, as shown in Figure 1c. The hot-air return was similar to that in Case 1. In Case 4 (overhead duct supply/HAC return), the air supply was the same as that in Case 3; the main difference is that the

HAC between two adjacent rack rows is designed to directly transfer hot air to the CRAC, as shown in Figure 1d. The detailed parameters are listed in Table 2.

The cooling capacity of the CRAC can be adjusted to ensure that the average temperature of all racks (T_{avg}) is maintained at 23 °C for a specific rack power density [28], based on which the thermal performance is compared for different technologies. Subsequently, an economic analysis was conducted according to the different cooling capacities of the CRAC and FC strategies, whose performance in five major cities in China (namely, Harbin, Beijing, Shanghai, Xi'an, and Shenzhen) were analyzed. According to the supply air temperature (SAT) and ambient temperature (T_{amb}), there are three operating models: (1) mechanical cooling: $T_{amb-min} > SAT$, where the operating time of the refrigeration system is considered as 24 h per day; (2) partial free cooling: $T_{amb-min} < SAT < T_{amb-max}$, where the operating time of the refrigeration system is considered as 12 h per day; and (3) FC: $T_{amb-max} < SAT$, where the operating time of the refrigeration system is considered as 0 h per day [29]. Figure 2 shows the one-year temperature variation for the different operation models.
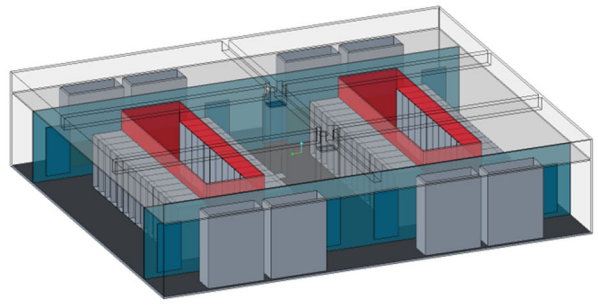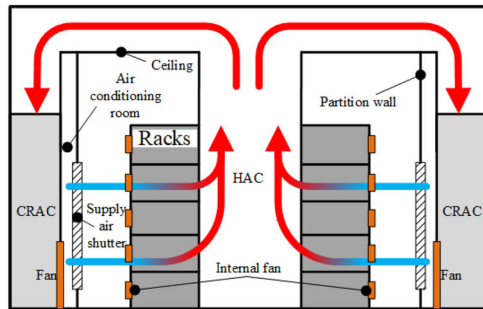
Governing equations

FloEFD software was used to establish a 3D model and study the DC performance. The continuity, momentum, and energy equations can be expressed as follows [30]:

$$\frac{\partial(\rho u)}{\partial x} + \frac{\partial(\rho v)}{\partial y} + \frac{\partial(\rho w)}{\partial z} = 0 \tag{1}$$
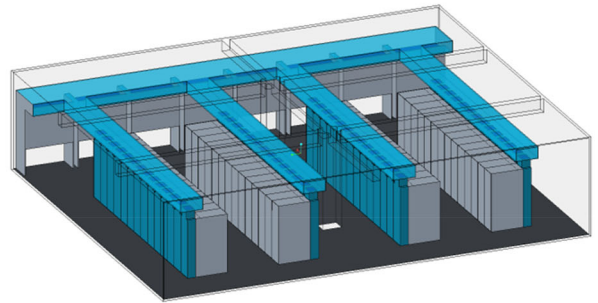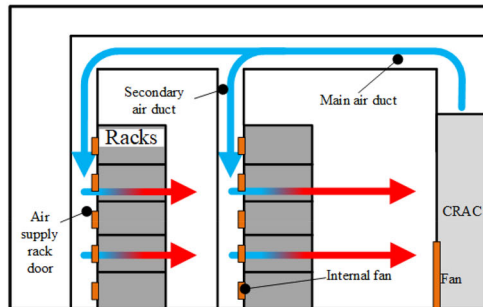
$$\begin{cases} \rho\left(u\frac{\partial u}{\partial x} + v\frac{\partial u}{\partial y} + w\frac{\partial u}{\partial z}\right) = \rho g_x - \frac{\partial P}{\partial x} + \mu\left(\frac{\partial^2 u}{\partial x^2} + \frac{\partial^2 u}{\partial y^2} + \frac{\partial^2 u}{\partial z^2}\right) + S_x \\ \rho\left(u\frac{\partial v}{\partial x} + v\frac{\partial v}{\partial y} + w\frac{\partial v}{\partial z}\right) = \rho g_y - \frac{\partial P}{\partial y} + \mu\left(\frac{\partial^2 v}{\partial x^2} + \frac{\partial^2 v}{\partial y^2} + \frac{\partial^2 v}{\partial z^2}\right) + S_y \\ \rho\left(u\frac{\partial w}{\partial x} + v\frac{\partial w}{\partial y} + w\frac{\partial w}{\partial z}\right) = \rho g_z - \frac{\partial P}{\partial z} + \mu\left(\frac{\partial^2 w}{\partial x^2} + \frac{\partial^2 w}{\partial y^2} + \frac{\partial^2 w}{\partial z^2}\right) + S_z \end{cases} \tag{2}$$
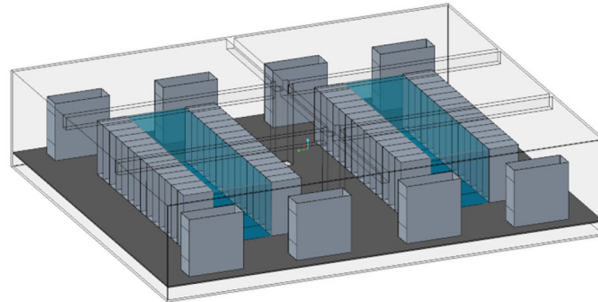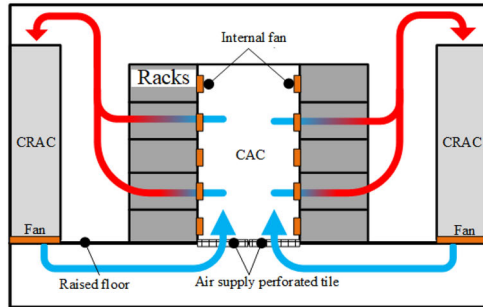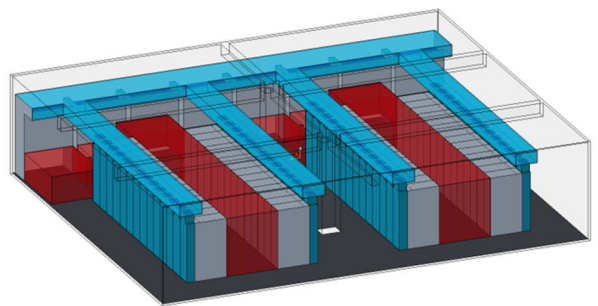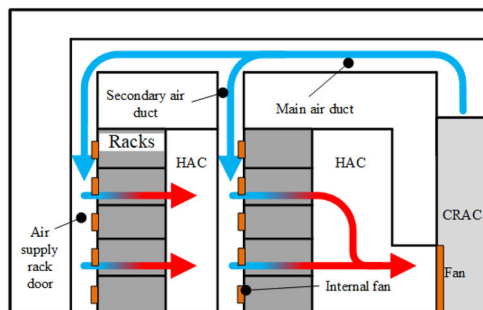

(a) Case 1: raised floor and CAC supply / CRAC direct return

(b) Case 2: CRAC direct supply / HAC return

(c) Case 3: Overhead duct supply / CRAC direct return

(d) Case 4: Overhead duct supply / HAC return

Figure 1. Schematic of the four airflow management technologies investigated in this study.

Table 2. Detailed parameters for DC room.

Items	Description	Case 1	Case 2	Case 3	Case 4
Room	L × W × H (m)		17.7 × 15 × 3.8		
Rack	L × W × H (m)		1.2 × 0.6 × 2		
	Numbers		56 (4 × 14)		
	Rack power (kW)		5–15		
Internal fan	D × H (m)		0.113 × 0.037		
	Number		5 × 2 (one rack)		
CRAC	L × W × H (m)		1.8 × 0.8 × 1.5		
	Number		8		
	Φ_0 (kW)		Depends on different rack power and case		
	V (m³/s)		4.2		
CAC	L × W × H (m)	8.4 × 2.38 × 2.2	–	–	–
Perforated tile	L × W (m)	1.2 × 1.2	–	–	–
Raised-floor	H (m)	0.6	–	–	–
HAC	L × W × H (m)	–	8.4 × 2.4 × 3	–	9.9 × 1.9 × 2.2
Main duct	L × W × H (m)	–	–	10.5 × 0.8 × 0.4	10.5 × 0.8 × 0.4
Secondary duct	L × W × H (m)	–	0.3 × 0.4 × 0.3	–	–
Shutter	W × H (m)	–	1 × 2	–	–
Rack door	L × W × H (m)	–	–	0.6 × 0.3 × 2.2	0.6 × 0.3 × 2.2
Ceiling	H (m)	–	3	–	–
Partition wall	W (m)	–	2	–	–

$$\frac{\partial(\rho u T)}{\partial x} + \frac{\partial(\rho v T)}{\partial y} + \frac{\partial(\rho w T)}{\partial z}$$
$$= \frac{\partial}{\partial x}\left(\frac{k}{c_p}\frac{\partial T}{\partial x}\right) + \frac{\partial}{\partial y}\left(\frac{k}{c_p}\frac{\partial T}{\partial y}\right) + \frac{\partial}{\partial z}\left(\frac{k}{c_p}\frac{\partial T}{\partial z}\right) + Q_H$$

$$(3)$$

where u, v, and w are the velocities in the x-, y-, and z-directions, respectively; ρ, g, P, and μ are the density, gravitational acceleration, pressure, and dynamic viscosity, respectively; S is the source term; T, k, and c_p are the temperature, thermal conductivity of the fluid, and specific heat capacity, respectively; and Q_H is the heat source per unit volume.

For simplicity, the porous media model employs the heat transfer and flow characteristics in the rack and CRAC, which can be expressed as [30]:

$$\begin{cases} S_i^{porous} = -R\delta_{ij}\rho u_i \\ Q_H^{porous} = \gamma(T_P - T_f) \end{cases} \quad (4)$$

where δ_{ij} is the Kronecker delta function (which is equal to unity when $i = j$, and zero otherwise); γ is the heat transfer coefficient of the working fluid; T_P and T_f are the temperatures of the porous matrix and fluid flowing through the matrix, respectively; and R is the resistance vector of the porous media, which can be calculated as follows:

$$R = \frac{A \cdot \Delta P}{L \cdot \dot{m}} \quad (5)$$

where A and L are the body cross-sectional area and length in the selected direction, respectively; ΔP is the pressure difference between the opposite

sides of a sample parallelepiped porous body; and $\dot{m}$ is the mass flow rate through the porous media.

Before the simulation, the following assumptions were made. (1) Steady-state is calculated, (2) the air is considered as an incompressible flow, (3) the rack power density is considered as a constant, and (4) the impact of radiation is ignored [31]. Based on these assumptions, the boundary conditions, model description, and solution method are determined, as listed in Table 3 [30, 32–36].

Performance indicators

Thermal performance indicators
To evaluate the DC thermal performance, SAT, temperature inequality index (K_T), supply heat index (SHI), and return heat index (RHI) are employed.

Normally, a high SAT can reduce energy consumption. In general, 10–35 °C is considered as the largest temperature range applied in DCs [37].

K_T evaluates the thermal environment of the rack from the temperature inequality level, which can be calculated as follows [38]:

$$K_T = \frac{1}{T_{avg}}\sqrt{\frac{\sum_{i=1}^{n}(T_{avg} - T_{i,j})^2}{n-1}} \quad (6)$$

where n is the total number of racks; $T_{i,j}$ is the temperature of the rack in row i and column j; and T_{avg} is the average temperature of all racks.

SHI and RHI indicate the size of the cooling capacity loss and the proportion of effective cooling capacity utilization in the total cooling capacity; a small

SHI value and a large RHI value indicate better thermal management. These can be calculated as follows [39]:

$$\begin{cases} SHI = \dfrac{\delta Q}{Q + \delta Q} = \dfrac{\sum j \sum i M_{i,j} c_p \left[(T_{in})_{i,j} - T_{sat} \right]}{\sum j \sum i M_{i,j} c_p \left[(T_{out})_{i,j} - T_{sat} \right]} \\ RHI = \dfrac{Q}{Q + \delta Q} = \dfrac{\sum j \sum i M_{i,j} c_p \left[(T_{out})_{i,j} - (T_{in})_{i,j} \right]}{\sum j \sum i M_{i,j} c_p \left[(T_{out})_{i,j} - T_{sat} \right]} \end{cases} \quad (7)$$

where Q and δQ represent the total heat dissipation of the DC racks and the enthalpy increase of cold air before entering the rack, respectively; i and j are the row and column coordinates of the enclosure, respectively; and $M_{i,j}$ represents the air mass flow of the rack in row i and column j.

Economic performance indicators

Using the simulation results, an economic analysis was conducted to compare the performance in
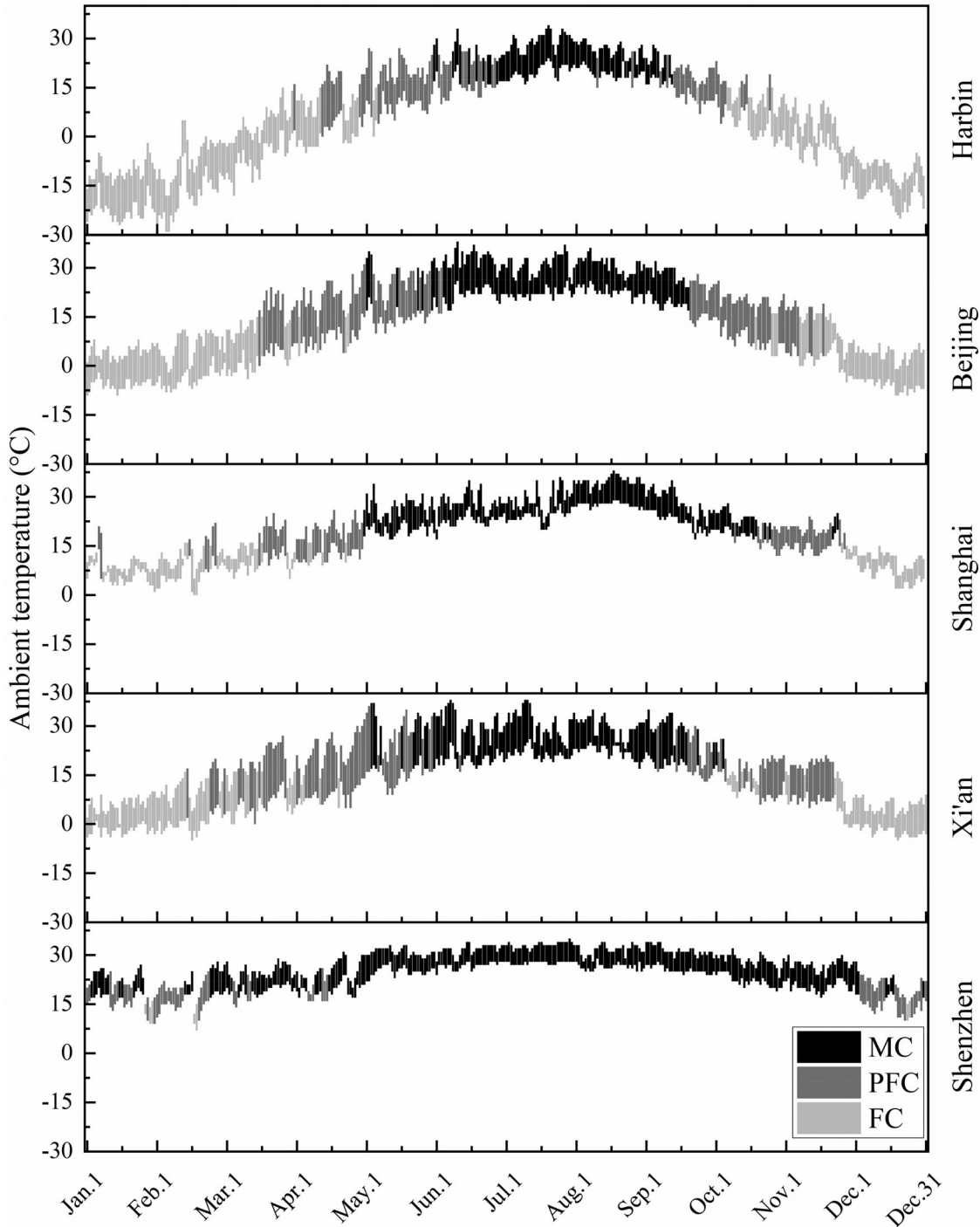

Figure 2. Annual ambient temperature variation according to the operation model for Case 1.

Table 3. Detailed simulation parameters and condition settings.

Type	Items	Settings
Boundary conditions	Rack	Power density: 5–15 kW; Internal fan is defined by characteristic curve [32, 33]; Porous media: Porosity: 0.5 [34]; Pressure loss: 300 Pa [32]; Body cross-sectional area and length: 1.29 m² and 1 m.
	CRAC	Heat source: <-35 kW; Internal fan: 4.2 m³/s; Porous media: Porosity: 0.965 [35]; Pressure loss: 0 Pa; Body cross-sectional area and length: 1.76 m² and 1.2 m.
	Perforated tile	Porous media: Porosity: 0.5 [33]; Pressure loss is defined by characteristic curve [33]; Body cross-sectional area and length: 1.44 m² and 0.05 m.
	Shutter	Single direction porous media: Porosity: 0.98 [36]; Pressure loss: 0 Pa; Body cross-sectional area and length: 2 m² and 0.05 m.
	Solid wall	Thermal insulation wall (No solid internal heat transfer)
	Working fluid	Air: Density, specific heat, and thermal conductivity were defined as a function of temperature [30].
	Initial state	Initial temperature: 23 °C; Initial velocity: 0 m/s.
Model	Turbulence model	Standard κ-ε model [30]: $\frac{\partial}{\partial x_i}(\rho u_i k) = \frac{\partial}{\partial x_j}\left[\left(\mu + \frac{\mu_t}{\sigma_\kappa}\right)\frac{\partial \kappa}{\partial x_j}\right] + G_\kappa + G_b - \rho\varepsilon$ $\frac{\partial}{\partial x_i}(\rho u_i \varepsilon) = \frac{\partial}{\partial x_j}\left[\left(\mu + \frac{\mu_t}{\sigma_\varepsilon}\right)\frac{\partial \varepsilon}{\partial x_j}\right] + C_{1\varepsilon}\frac{\varepsilon}{\kappa}(G_\kappa + C_{3\varepsilon}G_b) - C_{2\varepsilon}\frac{\rho\varepsilon^2}{\kappa}$ where i represents the x-, y- or z-axis; κ is turbulent pulsation kinetic energy; ε is the dissipation rate of turbulent pulsation kinetic energy; G_κ is the turbulent kinetic energy at the mean velocity gradient, $G_\kappa = \rho\overline{u_i u_j}\frac{\partial u_j}{\partial u_i}$; μ_t is the turbulent viscosity, $\mu_t = \rho C_\mu \frac{\kappa^2}{\varepsilon}$; G_b is the turbulent kinetic energy generated by buoyancy, $G_b = \beta g_i \frac{\mu_t}{Pr_t}\frac{\partial T}{\partial x_i}$; Pr is the Prandtl number, $Pr_t = 0.85$; β is the expansion coefficient, $\beta = -\frac{1}{\rho}\left(\frac{\partial\rho}{\partial T}\right)_P$; $C_{1\varepsilon}$, $C_{2\varepsilon}$, $C_{3\varepsilon}$, C_μ, σ_k and σ_ε are constants in the standard κ-ε model.
	Wall function	Two-Scales Wall Functions Model (including "thick-boundary-layer" and "thin-boundary-layer", they will be automatically selected according to the calculation mesh in the software FloEFD [30])
Solution	Pressure–Velocity coupling	SIMPLE
	Spatial discretization	Pressure: PRESTO!; Density, Momentum and Energy: Second Order Upwind.
	Residuals	Continuity and momentum: 1×10^{-3}; Energy: 1×10^{-6}

different cases and regions. Therefore, the energy consumption, power usage effectiveness (PUE), and annual cost value (ACV) are selected.

To calculate the energy consumption, the refrigeration system performance is required [40], as shown in Equation (8).

$$\begin{cases} P_{com} = q(h_1 - h_2) \\ q = \dfrac{\Phi 0}{h_1 - h_3} \end{cases} \tag{8}$$

where q, $\Phi 0$, and P_{com} represent the mass flow in the refrigerated system, the cooling capacity of a single CRAC, and the compressor energy consumption, respectively. h_1, h_2, and h_3 represent the enthalpy of the refrigerant at the compressor, condenser, and throttle valve inlets, respectively.

PUE is often used to quantitatively analyze the energy consumption utilization of DCs, which is defined as [41]:

$$\begin{cases} PUE = \dfrac{E_{total}}{E_{IT}} = \dfrac{E_{IT} + E_{CS} + E_{ES}}{E_{IT}} \\ E_{CS} = \eta n(P_{com})t_{total} \end{cases} \tag{9}$$

where E_{IT} is the rack energy consumption; E_{ES} includes the energy consumption of the uninterruptible power supply, lighting, security equipment, and office equipment, which is assumed to be 20% of E_{total} [42]; E_{CS} is the energy consumption of the refrigeration system; η is the load rate, which is considered to be 0.8 [41]; n represents the number of CRACs; and t_{total} represents the annual working time of the refrigeration system.

For the construction cost, the rack and CRAC costs are ignored, and only the cost related to airflow management is considered, as shown in Table 4 [43].

ACV is the value of the equipment life cycle, which comes from two parts [42]:

$$\begin{cases} ACV = \dfrac{b(1+b)^m}{b(1+b)^m - 1}C_{con} + C_{op} \\ C_{op} = fE_{CS} \end{cases} \tag{10}$$

where C_{con} is the construction cost, which comes from Table 4; C_{op} is the operational cost, which comes from Equations (8) and (9); b and m are the basic rate of return (6%) and economic life (10 years), respectively; and f is the average electricity price, which is calculated for different regions.

Grid independence test

Figure 3 shows the grid structure. To reduce the grid number and improve the accuracy of the results, the

grid is refined at the walls of the rack, CRAC, and fluid-solid coupling surface, as shown in Figure 3. Table 5 lists the grid-independence test results. It can be found that the average rack temperature and K_T varied less than $0.3\,°C$ and 1.1% when the grid number exceeded 7,269,482, 7,695,627, 8,078,638, and 8,363,886 for Cases 1–4, respectively. To reduce the calculation time, the appropriate grid number for each case was employed.

Table 4. Construction cost of different cases [43].

Item	Price (CNY)	Number			
		Case1	Case2	Case3	Case4
CAC	2000	2	—	—	—
HAC	2000	—	2	—	2
Perforated tile	200	112	—	—	—
Partition wall	40	—	270	—	135
Floor	100	626	—	—	—
Ceiling	35	—	626	—	—
Air duct	30	—	—	133	133
Supply shutter	480	—	8	—	—
Duct internal shutter	50	—	—	56	56
Labor cost	20	200	220	180	200
Total (CNY)		93000	44950	10390	20190

Model validation

To validate the proposed model, Abdelmaksoud's work [33] was employed, in which a raised floor air supply was adopted, as shown in Figure 4. The
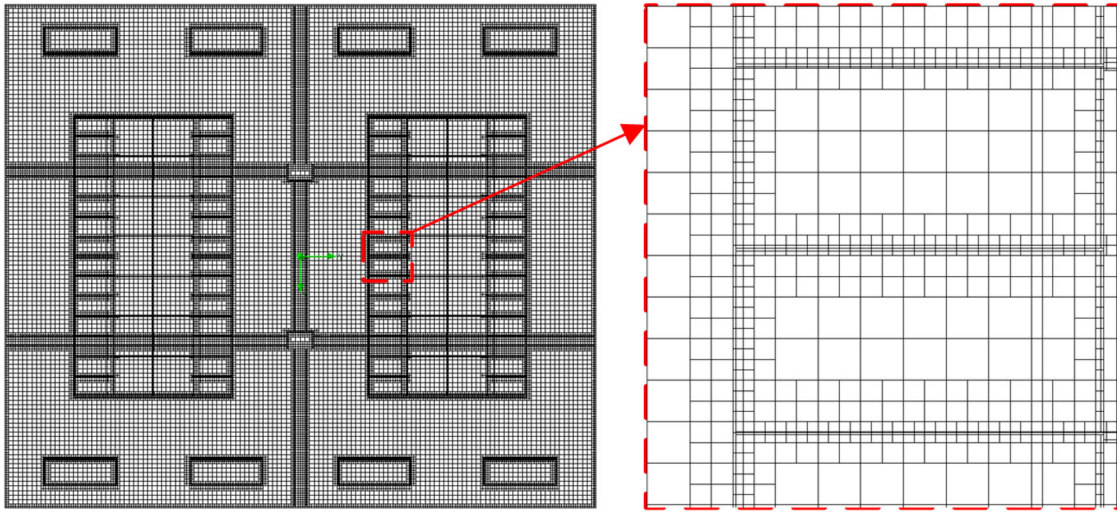

Figure 3. Grid structure details.

Table 5. Grid independence test.

Case	Number of grids	T_{avg} (°C)	T_{avg} deviation (°C)	K_T	K_T relative deviation (%)
Case 1	844,362	25.8	—	0.1964	—
	1,878,923	23.7	2.1	0.1262	35.7
	2,946,526	22.4	1.3	0.0939	25.6
	4,619,368	22.8	−0.4	0.0634	32.5
	7,269,482	23.0	−0.2	0.0474	25.3
	10,591,502	23.1	−0.1	0.0469	1.1
Case 2	953,626	25.7	—	0.2236	—
	1,986,548	23.7	2.0	0.1465	34.5
	3,123,963	22.3	1.4	0.1033	29.5
	4,965,684	22.8	−0.5	0.0870	15.8
	7,695,627	23.0	−0.2	0.0793	8.9
	11,936,581	23.0	0.0	0.0789	0.5
Case 3	1,023,983	25.7	—	0.1721	—
	2,297,774	22.4	3.3	0.1066	38.1
	4,541,126	23.2	−0.8	0.0612	42.6
	6,227,022	22.9	0.3	0.0472	22.9
	8,078,638	23.0	−0.1	0.0392	16.9
	12,926,445	23.0	0.0	0.0391	0.3
Case 4	1,475,262	25.1	—	0.1433	—
	2,429,765	22.5	2.6	0.0935	34.8
	4,059,649	23.4	−0.9	0.0624	33.3
	5,729,904	22.8	0.6	0.0492	21.1
	8,363,886	23.0	−0.2	0.0332	32.6
	13,532,488	23.1	−0.1	0.0330	0.4

experiment consists of one CRAC and three racks. The detailed parameters are listed in Table 6. The air supply, rack inlet, and rack outlet temperatures were monitored along the height direction. The temperature differences between the rack inlet and outlet and the SAT were used to validate the model, which can be calculated as follows:

$$\begin{cases} \Delta T^i_{in} = T^i_{in} - SAT \\ \Delta T^i_{out} = T^i_{out} - SAT \end{cases} \quad (11)$$

where T^i_{in} and T^i_{out} respectively represent the cabinet inlet and outlet temperatures at different heights.

The model validation is illustrated in Figure 5. The simulation results were in good agreement with the experimental data. The temperature deviation was less than $1\,°C$ for both the rack inlet and outlet (the rack height was $2\,m$), which is less than the maximum uncertainty in the experiment ($1.1\,°C$) and it may arise from the measurement deviation in the experiment. It should be noted that the uncertainty was directly obtained from Abdelmaksoud's work [33]. Therefore, the model was considered validated and suitable to predict the performance of different airflow management technologies.
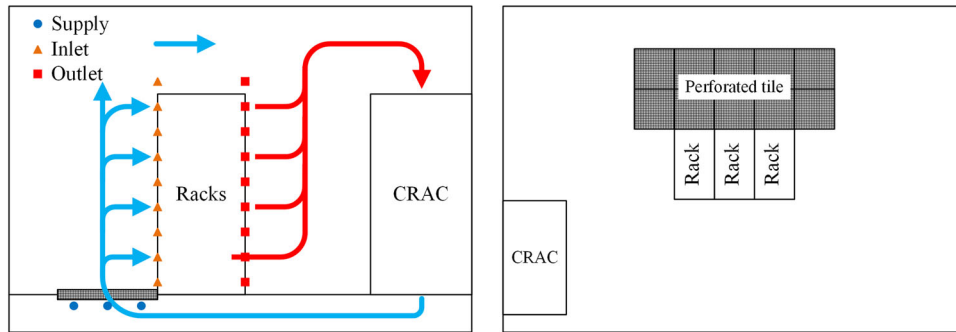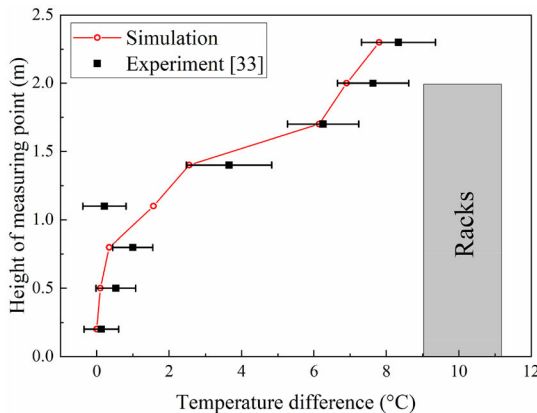

Figure 4. Experimental model arrangement in reference [33].

Table 6. Detailed parameters in the model.

Items	Description	Parameters
Room	L × W × H (m × m × m)	7.9 × 5.6 × 3.6
Perforated tile	L × W (m × m)	0.6 × 0.6
Rack	L × W × H (m × m × m)	1.2 × 0.6 × 2
	Number of racks	3
	Rack power (kW)	33.3
Internal fan	D × H (m)	0.113 × 0.037
	Number	8 × 2 (one rack)
CRAC	L × W × H (m × m)	1.8 × 0.8 × 2
	Number	1
	Single refrigerating capacity (kW)	100
	Single flow rate (m³/s)	4

(a) Validation at the rack inlet
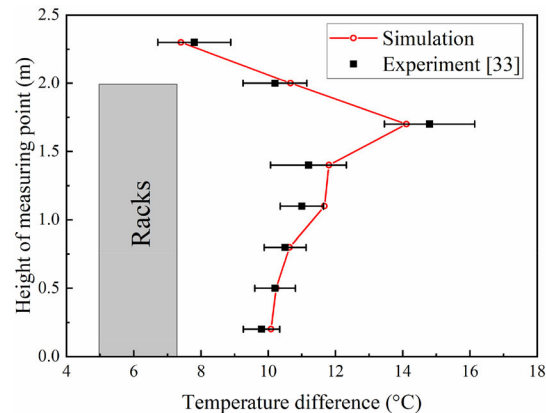
(b) Validation at the rack outlet

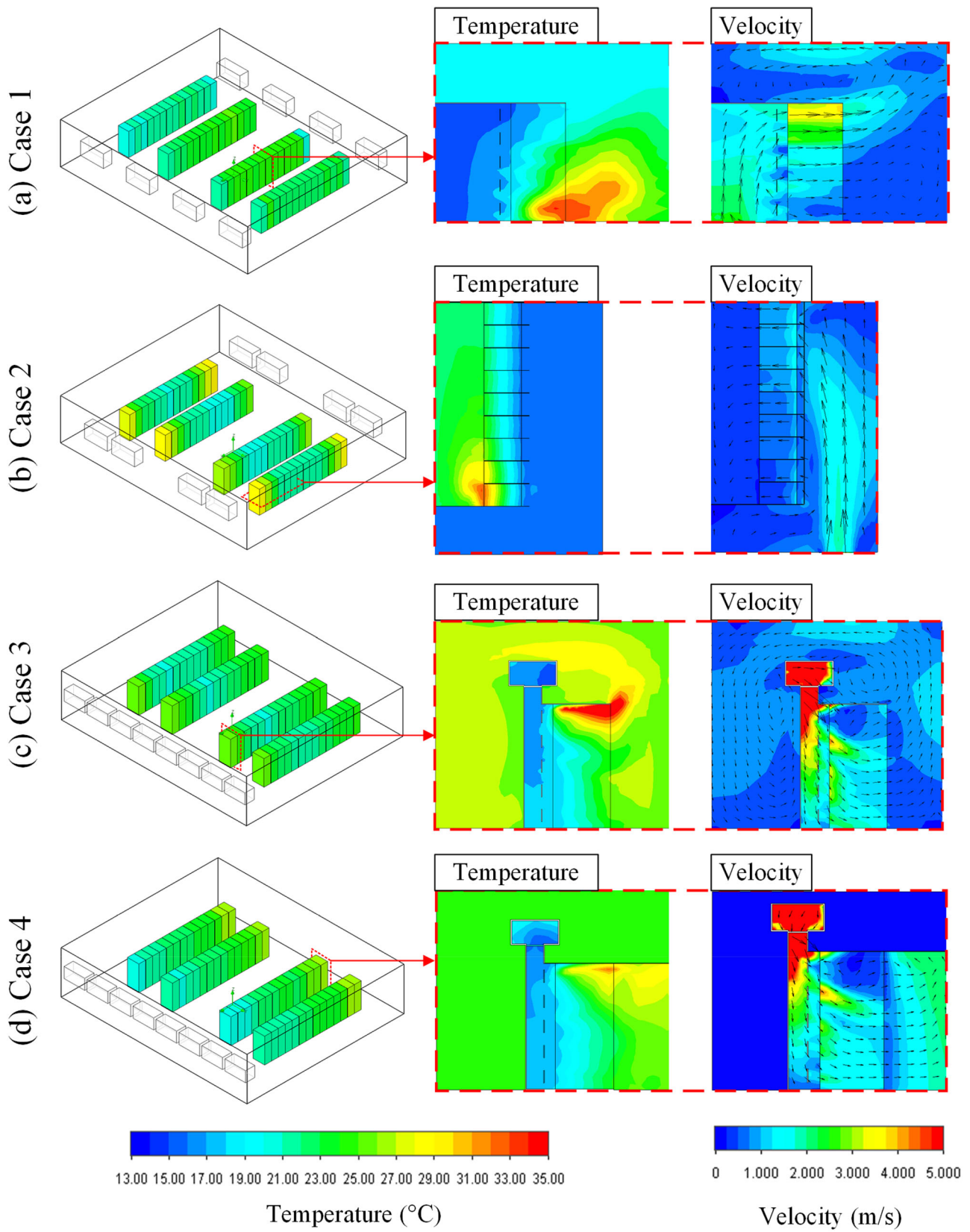**Figure 5.** Model validation results at the rack inlet and outlet.

Figure 6. Temperature and airflow distributions under a 10 kW rack power density.

Results and discussion

Thermal performance of different airflow management technologies

Figure 6 illustrates the thermal performance of different airflow management technologies at 10 kW, in which the temperature and velocity distributions are magnified for the hot pot region. Because of the different airflow configurations, the hot pot of the rack was also different. Generally, a hot pot occurs when the air velocity is low. For Case 1, because cold air was transferred from the perforated tile and the flow rate was higher at the top of the rack, the hot pot normally occurred at the bottom of the rack, as shown in Figure 6a. For Case 2, more cold air was found to flow into the rack in the middle of the row, leading to the hot pot occurring at both ends of the row, as shown in Figure 6b. Because an overhead air duct was used to supply cold air, a hot pot normally occurred at the top of the rack, as shown in Figure 6c,d. In addition, because of the HAC, the hot pot area in Case 4 was smaller than that in Case 3.

Figure 7 shows an SAT comparison between the different airflow management technologies, in which the average rack temperature was maintained at 23 °C. As can be seen, all four technologies could be employed when the rack power density was less than 10 kW. However, the SAT was different. For example, when the power density was 5 kW, the SATs were 16.9, 17.8, 17.1, and 19.5 °C for Cases 1–4, respectively. A high SAT indicates a low refrigeration system energy consumption. It can also be seen that because the SAT was lower than the minimum SAT recommended by ASHRAE (10 °C), Case 1 cannot meet the requirement when the rack power density is above 12.5 kW; whereas only Case 4 can be used when the rack power density exceeds 15 kW. Therefore, the airflow with an overhead duct supply and HAC return can obtain a higher SAT to achieve high thermal performance.

Figure 8 shows the temperature inequality index (K_T) results. With an increase in the rack power density, K_T also increased, indicating that there were more hot pots. Taking Case 2 as an example, K_T increased from 0.055 to 0.160 when the power density increased from 5 to 15 kW. For specific rack power densities, K_T in Case 4 was the smallest, followed by Cases 3, 1, and 2. This is because the hot spot caused by the airflow vortex can be avoided as much as possible by using an air duct and HAC. Therefore, the airflow should be carefully optimized if K_T is large.
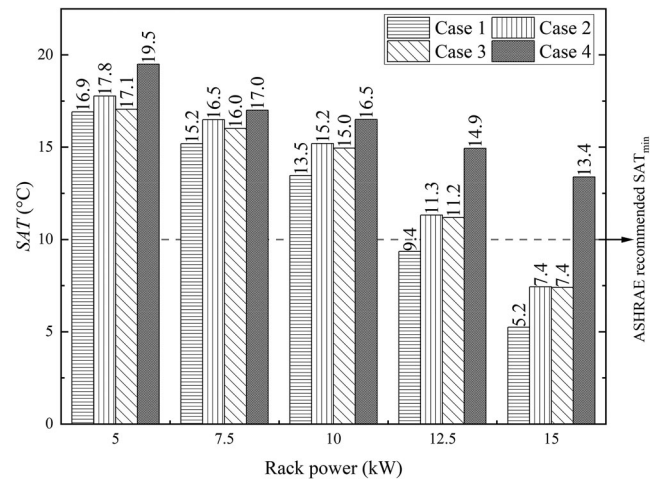

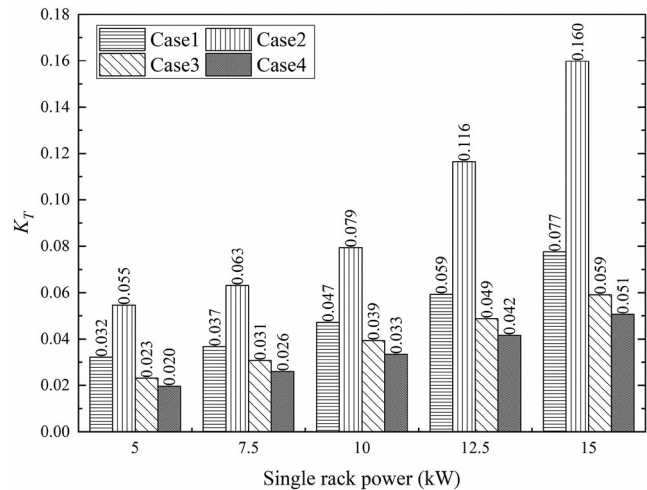**Figure 7.** SAT for Cases 1–4 under different rack power densities.

Figure 8. K_T variation for Cases 1–4 under different rack power densities.

Figure 9 shows the variations in SHI and RHI. Owing to the different airflow management technologies, Case 4 exhibited the highest RHI and lowest SHI, followed by Cases 3, 2, and 1 for the same rack power density, indicating that Case 4 had the smallest energy consumption loss. Case 4 outperformed the other cases mainly because of the following: (1) the cold air can be evenly distributed to every rack; (2) the cold and hot aisles were completely separated and there was no hot air recirculation. Taking the 5-kW power density as an example, RHI/SHI was 0.274/0.726, 0.226/0.774, 0.173/0.827, and 0.148/0.852 for Cases 1–4, respectively. In addition, SHI decreased and RHI increased with the increase in rack power density, which was mainly due to the large impact of hot air recirculation and heat exchange through the cold aisle. RHI/SHI changed to

0.281/0.719 when the power density was 15 kW for Case 1 (from 0.274/0.726 at 5 kW). Although the increased rack power density was detrimental to the thermal performance, Case 4 also exhibited the best performance.

Economic performance of different airflow management technologies

Figure 10 shows the annual refrigeration system energy consumption in different regions. Owing to
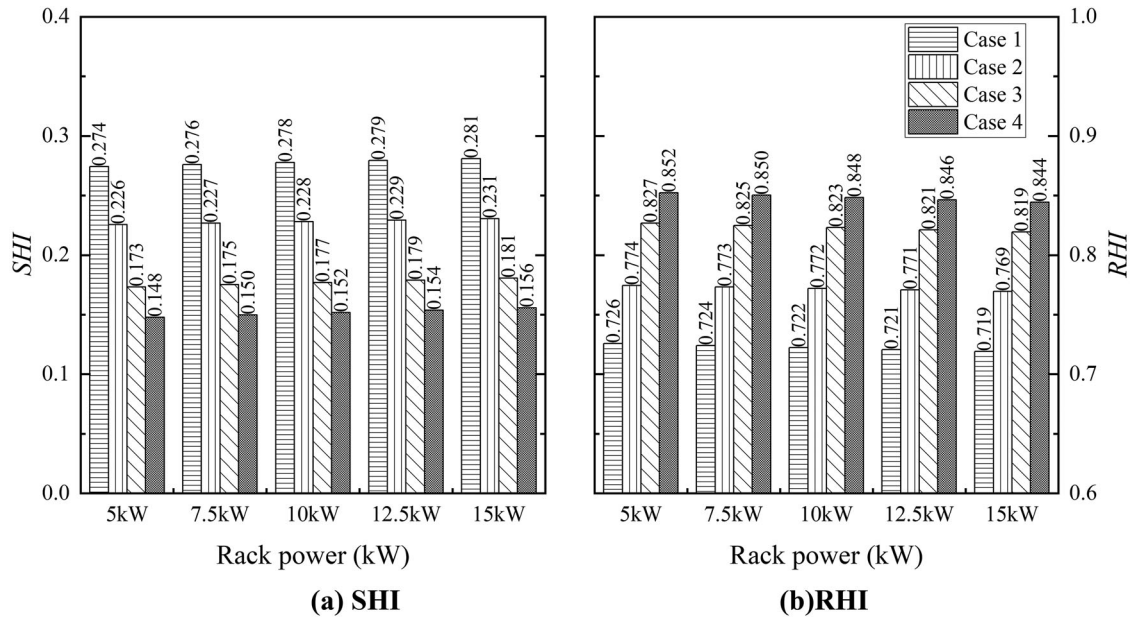

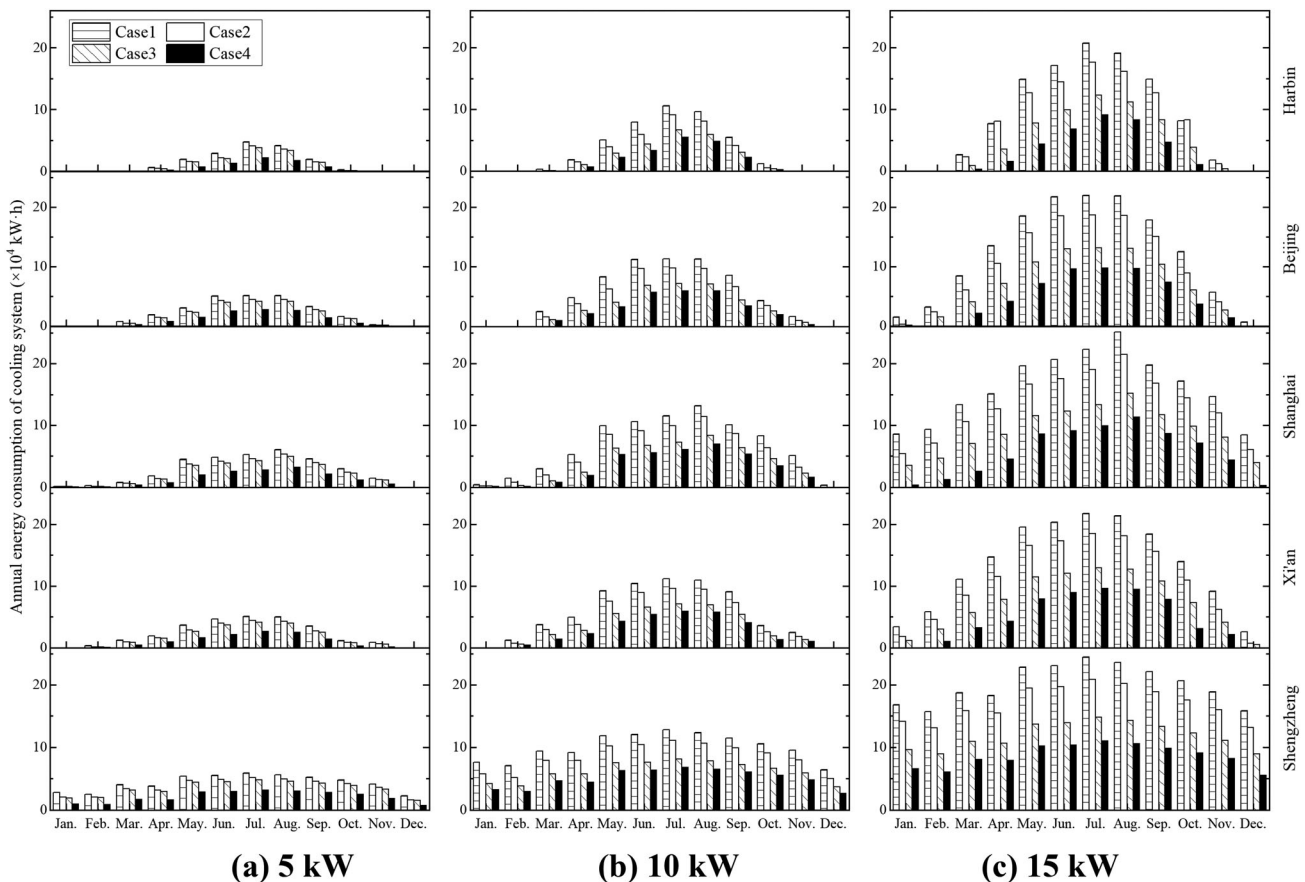**Figure 9.** SHI and RHI for Cases 1–4 under different rack power densities.

Figure 10. Annual energy consumption of the cooling system for Cases 1–4 according to region and rack power density.

the climate difference and FC strategy, the energy consumption in summer was higher than that in winter. Moreover, the energy consumption increased with an increase in rack power density. For different regions, the energy consumption was also significantly different. Shenzhen had the highest annual energy consumption, followed by Shanghai, Xi'an, Beijing, and Harbin. For example, when the power density was 10 kW, the energy consumption of Shenzhen was 64.95%, 66.89%, 66.90%, and 68.30% higher than that of Harbin for Cases 1–4, respectively. Owing to different airflow management technologies, the energy consumption also varied. Case 1 exhibited the highest energy consumption, followed by Cases 2, 3, and 4. Taking the 10-kW power density and Shenzhen as an example, the annual energy consumption of Case 4 was 602,486 kW·h, which is a reduction of up to 49.93%, 40.38%, and 18.81% compared to Cases 1, 2, and 3, respectively. The lowest energy consumption in Case 4 was due to the increased air supply temperature and its better thermal performance.

Figure 11 shows the variation in PUE for the different regions. As can be seen, owing to the increase in rack power density, PUE exhibited an increasing trend. For Beijing, when the rack power density increased from 5 to 15 kW, the PUE increased from 1.42, 1.39, 1.38, and 1.33 to 1.56, 1.50, 1.42 and 1.37 for Cases 1–4, respectively. Moreover, Harbin showed

the lowest PUE owing to the cold climate and FC strategy, followed by Beijing, Xi'an, Shanghai, and Shenzhen. More importantly, the PUE of Cases 1–4 changed slightly for a 5 kW power density; while it changed largely for a 15 kW power density. Therefore, these four cases can be applied to different regions when the power density is low. Case 4 is recommended for a high rack power density.

Figure 12 shows the cooling system ACV results for the different cases according to region. It is clear that ACV increased with an increase in rack power density. It was also significantly affected by climate. In Beijing, the ACV was 17.39×10^5 CNY for Case 1 at 5 kW, while it increased to 23.72×10^5 CNY when the power density was 15 kW. Moreover, the annual cost largely varied for different regions when the power density increased to 15 kW; the ACV of Case 1 in Harbin, Beijing, Shanghai, Xi'an, and Shenzhen were 23.27×10^5, 23.72×10^5, 27.00×10^5, 24.78×10^5, and 28.97×10^5 CNY, respectively. Owing to the difference in the capital cost and thermal performance, the annual cost of Case 3 was the lowest when the power density was 5 kW, followed by Cases 4, 2, and 1. However, Case 4 exhibited the lowest annual cost in Shanghai, Xi'an, and Shenzhen when the power density reached 15 kW, which was mainly due to the high thermal performance, which in turn results in a better economic performance, in regions with high ambient temperatures.
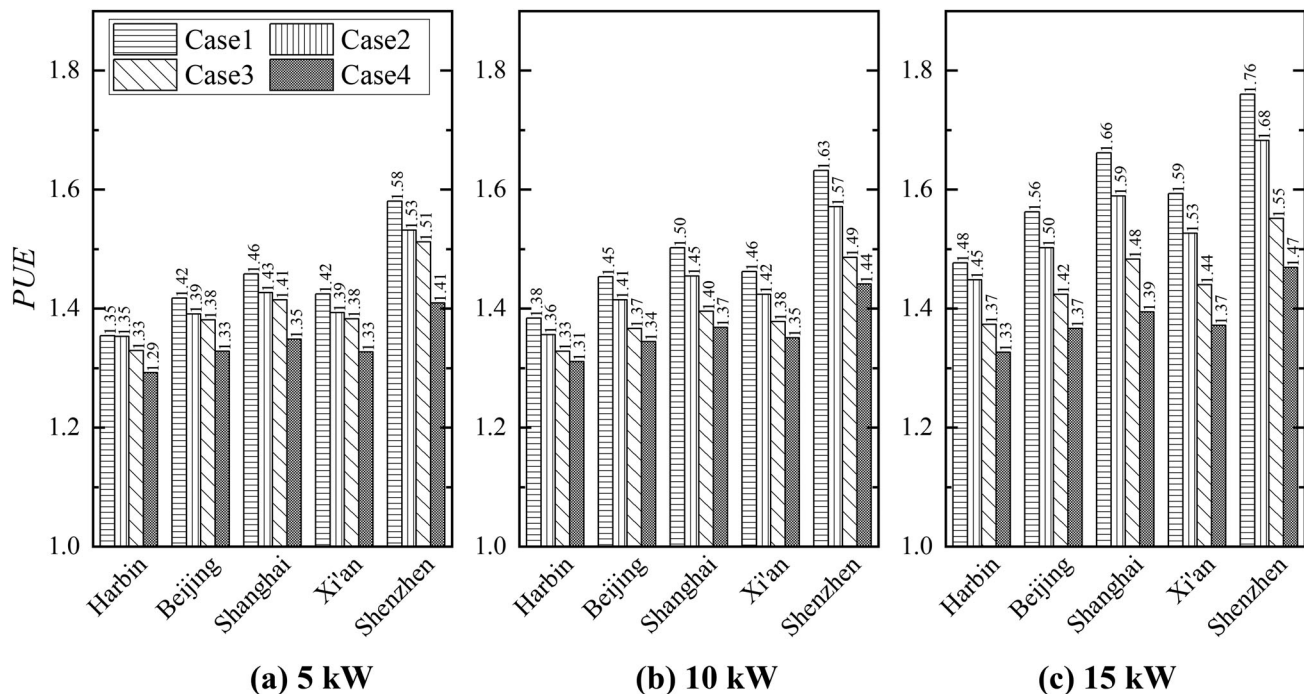

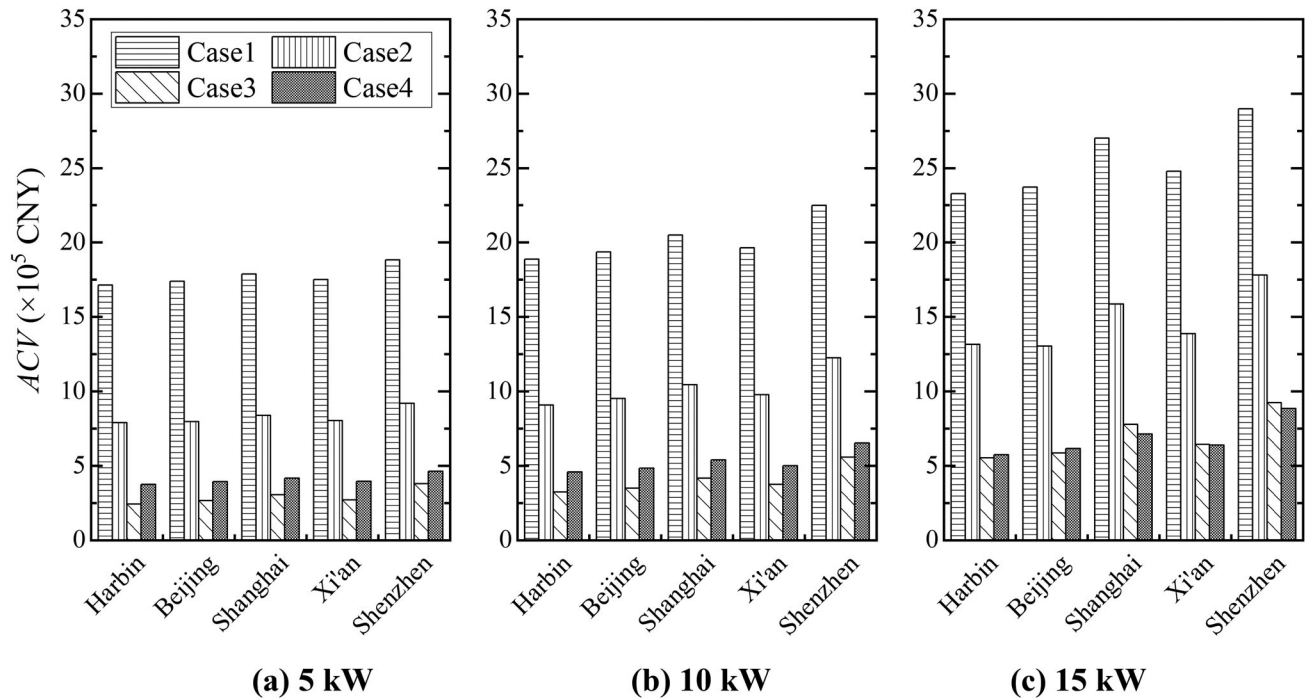**Figure 11.** *PUE* for Cases 1–4 according to region and rack power density.

Figure 12. Annual cost for Cases 1–4 according to region and rack power density.

Discussion

In this study, the thermal and economic performances of four airflow management technologies were compared. Based on the results, an optimal structure is suggested. However, this study compared their performance without considering optimization. Optimization is also an effective way to improve the performance of airflow management technologies, which we will investigate in future work. The hot pot and temperature inequality index are illustrated in this paper, which could provide guidance for optimization at high power densities.

Conclusions

Air cooling technology, which has the advantages of low capital cost, high reliability, and simple structure, is the most common method used in DCs. With the increase in rack power density, airflow management technology needs to be upgraded. There are different airflow management technologies in current DCs. The optimal technology and its economic analysis should be carefully discussed to achieve a high rack power density. Therefore, this study compared the thermal and economic performances of four airflow management technologies, which was helpful in selecting a suitable cooling method at a high rack power density. These four technologies included the following: Case 1: raised floor and CAC supply/CRAC direct return; Case 2: CRAC direct supply/HAC return; Case 3: overhead duct supply/CRAC direct return; and Case 4:

overhead duct supply/HAC return. Based on the results, it can be concluded that: (1) owing to the application of overhead duct supply and HAC return, Case 4 exhibited the highest SAT and RHI and the lowest K_T and SHI, followed by Cases 3, 2, and 1. For a 15-kW power density, the SATs/RHIs were 13.4 °C/0.844, 7.4 °C/0.819, 7.4 °C/0.769, and 5.2 °C/0.719 for Cases 1–4, respectively. (2) Because the SAT was lower than the minimum SAT recommended by ASHRAE (10 °C), Case 1 cannot meet the heat dissipation requirement when the rack power density exceeds 12.5 kW; whereas only Case 4 can be used when the rack power density exceeds 15 kW. (3) Owing to the high ambient temperature, Shenzhen exhibited the highest annual cost value (ACV) and power usage effectiveness (PUE), followed by Shanghai, Xi'an, Beijing, and Harbin. Furthermore, Cases 3 and 4 are recommended for application when the rack power density exceeds 10 kW.

Disclosure statement

The authors declare that they have no known competing financial interests or personal relationships that could have influenced the work reported in this paper.

Funding

Notes on contributors

Xueqiang Li is a lecturer in the School of Mechanical Engineering, Tianjin University of Commerce, China. He received his Ph.D. in Thermal Engineering from Tianjin University in 2019. His research focuses on the enhancement of heat transfer.

Zhongyao Zhang is a postgraduate at the School of Mechanical Engineering, Tianjin University of Commerce, China. He obtained her bachelor's degree in Energy and Power Engineering Talents from Tianjin University of Commerce in 2021.

Qihui Wang is an undergraduate student at the School of Mechanical Engineering, Tianjin University of Commerce, China.

Xiaohu Yang is a full professor in the School of Human Settlements and Civil Engineering, Xi'an Jiaotong University, China. He received his Ph.D. in Energy and Power Engineering from Xi'an Jiaotong University in 2015. His research focuses on the enhancement of heat transfer and energy savings in building.

Kamel Hooman is a professor in the Department of Process and Energy (P&E), Delft University of Technology, Delft, Nederland. His research focuses on the enhancement of heat transfer in thermal applications, energy savings, thermodynamics, and district heating.

Shengchun Liu a full professor in the School of Mechanical Engineering, Tianjin University of Commerce, China. He received his Ph.D. in Thermal Engineering from Tianjin University in 2006. His research focuses on the enhancement of heat transfer, design, and optimization of refrigeration system.

References

[1] A. A. Sbaity, H. Louahlia and S. Le Masson, "Performance of a hybrid thermosyphon condenser for cooling a typical data center under various climatic constraints," *Appl. Therm. Eng.*, vol. 202, pp. 117786, Feb. 2022. DOI: 10.1016/j.applthermaleng.2021.117786.

[2] Z. Li and S. G. Kandlikar, "Current status and future trends in data center cooling technologies," *Heat Transfer Eng.*, vol. 36, no. 6, pp. 523–538, 2015. DOI: 10.1080/01457632.2014.939032.

[3] J.-M. Pierson, et al., "DATAZERO: DATA center with zero emission and robust management using renewable energy," *IEEE Access*, vol. 7, pp. 103209–103230, Jul. 2019. DOI: 10.1109/ACCESS.2019.2930368.

[4] A. S. G. Andrae and T. Edler, "On global electricity usage of communication technology: trends to 2030," *Challenges*, vol. 6, no. 1, pp. 117–157, Apr. 2015. DOI: 10.3390/challe6010117.

[5] A. Haywood, J. Sherbeck, P. Phelan, G. Varsamopoulos and S. K. S. Gupta, "Thermodynamic feasibility of harvesting data center waste heat to drive an absorption chiller," *Energy Convers. Manage.*, vol. 58, pp. 26–34, Jun. 2012. DOI: 10.1016/j.enconman.2011.12.017.

[6] S.-M. Lin, et al., "Optimum design and heat transfer correlation equation of a mini radiator with jet impingement cooling," *Appl. Therm. Eng.*, vol. 89, pp. 727–737, Oct. 2015. DOI: 10.1016/j.applthermaleng.2015.06.065.

[7] M. Ruiz, C. M. Kunkle, J. Padilla and V. P. Carey, "Boiling heat transfer performance in a spiraling radial inflow microchannel cold plate," *Heat Transfer Eng.*, vol. 38, no. 14–15, pp. 1247–1259, 2017. DOI: 10.1080/01457632.2016.1242954.

[8] M. A. Kadhim, N. Kapur, J. L. Summers and H. Thompson, "Rack level study of hybrid liquid/air cooled servers: the impact of flow distribution and pumping configuration on central processing units temperature," *Heat Transfer Eng.*, vol. 41, no. 19–20, pp. 1683–1698, 2020. DOI: 10.1080/01457632.2019.1640467.

[9] A. H. Khalaj and S. K. Halgamuge, "A Review on efficient thermal management of air- and liquid-cooled data centers: from chip to the cooling system," *Appl. Energy*, vol. 205, pp. 1165–1188, Nov. 2017. DOI: 10.1016/j.apenergy.2017.08.037.

[10] V. K. Arghode, V. Sundaralingam and Y. Joshi, "Airflow management in a contained cold aisle using active fan tiles for energy efficient data-center operation," *Heat Transfer Eng.*, vol. 37, no. 3–4, pp. 246–256, 2016. DOI: 10.1080/01457632.2015.1051386.

[11] C.-H. Wang, Y.-Y. Tsui and C.-C. Wang, "On cold-aisle containment of a container datacenter," *Appl. Therm. Eng.*, vol. 112, pp. 133–142, Feb. 2017. DOI: 10.1016/j.applthermaleng.2016.10.089.

[12] C.-H. Wang, Y.-Y. Tsui and C.-C. Wang, "Airflow management on the efficiency index of a container data center having overhead air supply," *J. Electron.*

Packag., vol. 139, no. 4, pp. 041008, Dec. 2017. DOI: 10.1115/1.4038114.

[13] A. M. Abbas, A. S. Huzayyin, T. A. Mouneer and S. A. Nada, "Effect of data center servers' power density on the decision of using in-row cooling or perimeter cooling," *Alex. Eng. J.*, vol. 60, no. 4, pp. 3855–3867, Aug. 2021. DOI: 10.1016/j.aej.2021.02.051.

[14] H. M. Daraghmeh and C. C. Wang, "A review of current status of free cooling in data centers," *Appl. Therm. Eng.*, vol. 114, pp. 1224–1239, Mar. 2017. DOI: 10.1016/j.applthermaleng.2016.10.093.

[15] S.-W. Ham, M.-H. Kim, B.-N. Choi and J.-W. Jeong, "Energy saving potential of various air-side economizers in a modular data center," *Appl. Energy*, vol. 138, pp. 258–275, Jan. 2015. DOI: 10.1016/j.apenergy.2014.10.066.

[16] S.-W. Ham and J.-W. Jeong, "Impact of aisle containment on energy performance of a data center when using an integrated water-side economizer," *Appl. Therm. Eng.*, vol. 105, pp. 372–384, Jul. 2016. DOI: 10.1016/j.applthermaleng.2015.05.069.

[17] M. Zhang, et al., "Effect of raised floor height on different arrangement of under-floor air distribution performance in data center," *Procedia Eng.*, vol. 205, pp. 556–564, 2017. DOI: 10.1016/j.proeng.2017.10.425.

[18] S. A. Nada, K. E. Elfeky, A. M. A. Attia and W. G. Alshaer, "Experimental parametric study of servers cooling management in data centers buildings," *Heat Mass Transfer.*, vol. 53, no. 6, pp. 2083–2097, Jan. 2017. DOI: 10.1007/s00231-017-1966-y.

[19] Y. Fulpagare, G. Mahamuni and A. Bhargav, "Effect of plenum chamber obstructions on data center performance," *Appl. Therm. Eng.*, vol. 80, pp. 187–195, Apr. 2015. DOI: 10.1016/j.applthermaleng.2015.01.065.

[20] S. A. Nada and M. A. Said, "Effect of CRAC units layout on thermal management of data center," *Appl. Therm. Eng.*, vol. 118, pp. 339–344, May 2017. DOI: 10.1016/j.applthermaleng.2017.03.003.

[21] S. A. Nada, M. A. Said and M. A. Rady, "Numerical investigation and parametric study for thermal and energy management enhancements in data centers' buildings," *Appl. Therm. Eng.*, vol. 98, pp. 110–128, Apr. 2016. DOI: 10.1016/j.applthermaleng.2015.12.020.

[22] S. A. Nada, M. A. Said and M. A. Rady, "CFD investigations of data centers' thermal performance for different configurations of CRACs units and aisles separation," *Alex. Eng. J.*, vol. 55, no. 2, pp. 959–971, Jun. 2016. DOI: 10.1016/j.aej.2016.02.025.

[23] W. X. Chu, C. S. Hsu, Y. Y. Tsui and C. C. Wang, "Experimental investigation on thermal management for small container data center," *J. Build. Eng.*, vol. 21, pp. 317–327, Jan. 2019. DOI: 10.1016/j.jobe.2018.10.031.

[24] N. Srinarayana, B. Fakhim, M. Behnia and S. W. Armfield, "Thermal performance of an air-cooled data center with raised-floor and non-raised-floor configurations," *Heat Transfer Eng.*, vol. 35, no. 4, pp. 384–397, 2014. DOI: 10.1080/01457632.2013.828559.

[25] K. Nemati, H. A. Alissa, B. T. Murray and B. Sammakia, "Steady-state and transient comparison of cold and hot aisle containment and chimney,"

presented at The 15th IEEE Intersociety Conference on Thermal and Thermomechanical Phenomena in Electronic Systems (ITherm), Las Vegas, NV, USA, pp. 1435–1443, Jul. 2016. DOI: 10.1109/ITHERM.2016.7517717.

[26] B. Zhan, et al., "Experimental investigation on ducted hot aisle containment system for racks cooling of data center," *Int. J. Refrig.*, vol. 127, pp. 137–147, Jul. 2021. DOI: 10.1016/j.ijrefrig.2021.02.006.

[27] S. K. Shrivastava, A. R. Calder and M. Ibrahim, "Quantitative Comparison of Air Containment Systems," presented at," The 13th InterSociety Conference on Thermal and Thermomechanical Phenomena in Electronic Systems, San Diego, CA, USA, pp. 68–77, Jul. 2012. DOI: 10.1109/ITHERM.2012.6231415.

[28] Ashrae Technical Committee, *ASHRAE Datacom Series Book 1: Thermal Guidelines for Data Processing Environments*, 4th ed, American Society of Heating, Refrigerating and Air-Conditioning Engineers Inc, Atlanta, Georgia, USA, 2015,

[29] J. Gao, J. F. Zhang, Q. Y. Pan and C. H. Xia, "Design and application of intelligent out-door air system for data center in Guizhou information park," *J. HV&AC* vol. 46, no. 10, pp. 27–32, Oct. 2016. Available: https://kns.cnki.net/kcms/detail/detail.aspx?FileName=NTKT201610007&DbName=CJFQ2016.

[30] SIEMENS, "Simcenter FLOEFD^TM for Creo, Technical Reference, Software Version 2020.2," 2020. https://www.plm.automation.siemens.com/global/en/products/simcenter/floefd.html. Accessed: Dec. 6, 2022.

[31] J. Ni, B. Jin, B. Zhang and X. Wang, "Simulation of Thermal Distribution and Airflow for Efficient Energy Consumption in a Small Data Centers," *Sustainability*, vol. 9, no. 4, pp. 664, Apr. 2017. DOI: 10.3390/su9040664.

[32] J. F. Smith, *et al.*, "Design of Simulated Server Racks for Data Center Research," presented at," ASME 2011 Pacific Rim Technical Conference and Exhibition on Packaging and Integration of Electronic and Photonic Systems, Portland, Oregon, USA, vol. 2, pp. 415–422, Feb. 2012. DOI: 10.1115/IPACK2011-52016.

[33] W. A. Abdelmaksoud, "Experimental and Numerical Investigations of the Thermal Environment in Air-cooled Data Centers," Ph.D. dissertation, Syracuse University, New York, USA, 2012.

[34] D. V. Sheth and S. K. Saha, "Numerical study of thermal management of data centre using porous medium approach," *J. Build. Eng.*, vol. 22, pp. 200–215, Mar. 2019. DOI: 10.1016/j.jobe.2018.12.012.

[35] X. Ma, Q. Zhang, J. Wang and Y. Yu, "A coupled CFD approach for performance prediction of fin-and-tube condenser," *Numer. Heat Tr. A-Appl.*, vol. 78, no. 6, pp. 215–230, Jul. 2020. DOI: 10.1080/10407782.2020.1787057.

[36] A. Laouadi, "Thermal performance modelling of complex fenestration systems," *J. Build. Perform. Simu.*, vol. 2, no. 3, pp. 189–207, Sep. 2009. DOI: 10.1080/19401490903046785.

[37] S.-W. Ham, J.-S. Park and J.-W. Jeong, "Optimum supply air temperature ranges of various air-side

economizers in a modular data center," *Appl. Therm. Eng.*, vol. 77, pp. 163–179, Feb. 2015. DOI: 10.1016/j.applthermaleng.2014.12.021.

[38]   ASHRAE Technical Committee., *Thermal Guidelines for Data Processing Environments*, 3rd ed., American Society of Heating, Refrigerating and Air-Conditioning Engineers Inc, Atlanta, Georgia, USA, 2012

[39]   R. K. Sharma, C. E. Bash and C. D. Patel, "Dimensionless parameters for evaluation of thermal design and performance of large-scale data centers," presented at the," 8th AIAA/ASME Joint Thermophysics and Heat Transfer Conference, St. Louis, Missouri, USA, Jun. 2002. AIAA-2002-3091. DOI: 10.2514/6.2002-3091.

[40]   T. Miyazaki, B. B. Saha and S. Koyama, "Analytical Model of a Combined Adsorption Cooling and Mechanical Vapor Compression Refrigeration System," *Heat Transfer Eng.*, vol. 38, no. 4, pp. 423–430, 2017. DOI: 10.1080/01457632.2016.1195135.

[41]   N. Rasmussen, *Electrical efficiency modeling for data centers*. APC White Paper #113, American Power Conversion, USA. [Online]. Available: http://media.comtec.com/pdf/apc/ElectricalEfficiencyModelling.pdf. Accessed: Dec. 3, 2021.

[42]   S. B. Su, "Economic evaluation of cooling system construction in data center," Master dissertation, Harbin Institute of Technology, Harbin, China, 2019.

[43]   "Data center configuration list and quotation." [Online]. Available: https://wenku.baidu.com/view/8a9716d23086bceb19e8b8f67c1cfad6195fe906.html?fixfr=aQ%252BnMWzxsBnpstkFRriK%252Fg%253D%253D&fr=income4-wk_go_search-search. Accessed: Dec. 3, 2021.